Research Article | Vol. 24, No. 24 | 28 Nov 2016 | OPTICS EXPRESS 27425

Optics EXPRESS

Effect of non-conformal gold deposition on SERS related plasmonic effects

SWE ZIN OO* AND MARTIN D. B. CHARLTON

School of Electronics & Computer Science, University of Southampton, Southampton, SO17 1BJ, UK
**S.Oo@soton.ac.uk*

Abstract: Recently, a comprehensive three dimensional computational model based on rigorous coupled wave analysis (RCWA) has been developed to investigate the properties of surface plasmons resident on metal coated arrays of inverted pyramidal pits used for SERS sensing applications in the form of 'klarite'. This simulation tool allows the identification of a variety of dispersive features including propagating and localized surface plasmons as well as simple diffraction relating to the influence of geometrical features. In this paper, we investigate the influence of non-conformality of the gold coating over the internal surfaces of the inverted pyramidal pits on plasmon dispersion. Modeling reveals very strong changes in plasmon behavior as a function of gold layer conformality. Dependent upon conformality of the gold coating we find that the nano-textured metallic surface can behave either as an efficient broadband mirror-like reflector or as an efficient broadband, wide angle absorber at infrared wavelengths. Creation of a broadband wide angle absorbing surface such as this has important implications for photovoltaic cells. For sensing applications, understanding the effect of metal layer conformality on plasmon dispersion gives clear insight into how to further improve the SERS enhancement factor.

OCIS codes: (250.5403) Plasmonics; (240.6680) Surface plasmons; (240.6695) Surface-enhanced Raman scattering.

References and Links

1. N. M. B. Perney, F. J. García de Abajo, J. J. Baumberg, A. Tang, M. C. Netti, M. D. B. Charlton, and M. E. Zoorob, "Tuning Localized plasmon cavities for optimized surface-enhanced Raman scattering," Phys. Rev. B **76**(3), 035426 (2007).
2. T. M. Chinowsky, S. D. Soelberg, P. Baker, N. R. Swanson, P. Kauffman, A. Mactutis, M. S. Grow, R. Atmar, S. S. Yee, and C. E. Furlong, "Portable 24-analyte surface plasmon resonance instruments for rapid, versatile biodetection," Biosens. Bioelectron. **22**(9-10), 2268–2275 (2007).
3. S. Z. Oo, M. D. B. Charlton, D. Eustace, R. Y. Chen, S. J. Pearce, and M. E. Pollard, "Optimization of SERS enhancement from nanostructured metallic substrate based on arrays of inverted rectangular pyramids and investigation of effect of lattice non-symmetry," Proc. SPIE **8234**(823406), 1–7 (2012).
4. R. Colombelli, K. Srinivasan, M. Troccoli, O. Painter, C. F. Gmachl, D. M. Tennant, A. M. Sergent, D. L. Sivco, A. Y. Cho, and F. Capasso, "Quantum cascade surface-emitting photonic crystal laser," Science **302**(5649), 1374–1377 (2003).
5. R. F. Oulton, V. J. Sorger, T. Zentgraf, R.-M. Ma, C. Gladden, L. Dai, G. Bartal, and X. Zhang, "Plasmon lasers at deep subwavelength scale," Nature **461**(7264), 629–632 (2009).
6. M. T. Hill, Y. S. Oei, B. Smalbrugge, Y. Zhu, T. de Vries, P. J. van Veldhoven, F. W. M. van Otten, T. J. Eijkemans, J. P. Turkiewicz, H. de Waardt, E. J. Geluk, S. H. Kwon, Y. H. Lee, R. Notzel, and M. K. Smit, "Lasing in metallic-coated nanocavities," Nat. Photonics **1**(10), 589–594 (2007).
7. K. Okamoto, I. Niki, A. Shvartser, Y. Narukawa, T. Mukai, and A. Scherer, "Surface-plasmon-enhanced light emitters based on InGaN quantum wells," Nat. Mater. **3**(9), 601–605 (2004).
8. J. Müller, B. Rech, J. Springer, and M. Vanecek, "TCO and light trapping in silicon thin film solar cells," Sol. Energy **77**(6), 917–930 (2004).
9. S. Pillai, K. R. Catchpole, T. Trupke, and M. A. Green, "Surface plasmon enhanced silicon solar cells," J. Appl. Phys. **101**(9), 093105 (2007).
10. D. Derkacs, W. V. Chen, P. M. Matheu, S. H. Lim, P. K. L. Yu, and E. T. Yu, "Nanoparticle-induced light scattering for improved performance of quantum-well solar cells," Appl. Phys. Lett. **93**(9), 091107 (2008).
11. D. M. Schaadt, B. Feng, and E. T. Yu, "Enhanced semiconductor optical absorption via surface plasmon excitation in metal nanoparticles," Appl. Phys. Lett. **86**(6), 063106 (2005).

#267967 http://dx.doi.org/10.1364/OE.24.027425
Journal © 2016 Received 8 Jun 2016; revised 4 Jul 2016; accepted 4 Jul 2016; published 16 Nov 2016

Optics EXPRESS

12. K. Nakayama, K. Tanabe, and H. A. Atwater, "Plasmonic nanoparticle enhanced light absorption in GaAs solar cells," Appl. Phys. Lett. **93**(12), 121904 (2008).
13. D. Derkacs, S. H. Lim, P. Matheu, W. Mar, and E. T. Yu, "Improved performance of amorphous silicon solar cells via scattering from surface plasmon polaritons in nearby metallic nanoparticles," Appl. Phys. Lett. **89**(9), 093103 (2006).
14. P. Matheu, S. H. Lim, D. Derkacs, C. McPheeters, and E. T. Yu, "Metal and dielectric nanoparticle scattering for improved optical absorption in photovoltaic devices," Appl. Phys. Lett. **93**(11), 113108 (2008).
15. S. I. Bozhevolnyi, V. S. Volkov, E. Devaux, J. Y. Laluet, and T. W. Ebbesen, "Channel plasmon subwavelength waveguide components including interferometers and ring resonators," Nature **440**(7083), 508–511 (2006).
16. H. Ditlbacher, J. R. Krenn, G. Schider, A. Leitner, and F. R. Aussenegg, "Two-dimensional optics with surface plasmon polaritons," Appl. Phys. Lett. **81**(10), 1762–1764 (2002).
17. J. B. Pendry, "Negative refraction makes a perfect lens," Phys. Rev. Lett. **85**(18), 3966–3969 (2000).
18. R. Zia, M. D. Selker, P. B. Catrysse, and M. L. Brongersma, "Geometries and materials for subwavelength surface plasmon modes," J. Opt. Soc. Am. A **21**(12), 2442–2446 (2004).
19. A. F. Koenderink and A. Polman, "Complex response and polariton-like dispersion splitting in periodic metal nanoparticle chains," Phys. Rev. B **74**(3), 033402 (2006).
20. S. A. Maier, P. G. Kik, H. A. Atwater, S. Meltzer, E. Harel, B. E. Koel, and A. A. G. Requicha, "Local detection of electromagnetic energy transport below the diffraction limit in metal nanoparticle plasmon waveguides," Nat. Mater. **2**(4), 229–232 (2003).
21. M. Quinten, A. Leitner, J. R. Krenn, and F. R. Aussenegg, "Electromagnetic energy transport via linear chains of silver nanoparticles," Opt. Lett. **23**(17), 1331–1333 (1998).
22. P. Mühlschlegel, H. J. Eisler, O. J. F. Martin, B. Hecht, and D. W. Pohl, "Resonant optical antennas," Science **308**(5728), 1607–1609 (2005).
23. F. Bonaccorso, Z. Sun, T. Hasan, and A. C. Ferrari, "Graphene Photonics and Optoelectronics," Nat. Photonics **4**(9), 611–622 (2010).
24. F. Schedin, E. Lidorikis, A. Lombardo, V. G. Kravets, A. K. Geim, A. N. Grigorenko, K. S. Novoselov, and A. C. Ferrari, "Surface-Enhanced Raman Spectroscopy of Graphene," ACS Nano **4**(10), 5617–5626 (2010).
25. K. D. Osberg, M. Rycenga, N. Harris, A. L. Schmucker, M. R. Langille, G. C. Schatz, and C. A. Mirkin, "Dispersible Gold Nanorod Dimers with Sub-5 nm Gaps as Local Amplifiers for Surface-Enhanced Raman Scattering," Nano Lett. **12**(7), 3828–3832 (2012).
26. A. M. Gabudean, M. Focsan, and S. Astilean, "Gold Nanorods Performing as Dual-Modal Nanoprobes via Metal-Enhanced Fluorescence (MEF) and Surface-Enhanced Raman Scattering (SERS)," J. Phys. Chem. C **116**(22), 12240–12249 (2012).
27. D. Correia-Ledo, K. F. Gibson, A. Dhawan, M. Couture, T. Vo-Dinh, D. Graham, and J.-F. Masson, "Assessing the Location of Surface Plasmons Over Nanotriangle and Nanohole Arrays of Different Size and Periodicity," J Phys Chem C Nanomater Interfaces **116**(12), 6884–6892 (2012).
28. C. Steuwe, C. F. Kaminski, J. J. Baumberg, and S. Mahajan, "Surface Enhanced Coherent Anti-Stokes Raman Scattering on Nanostructured Gold Surfaces," Nano Lett. **11**(12), 5339–5343 (2011).
29. C. Tian, C. Ding, S. Liu, S. Yang, X. Song, B. Ding, Z. Li, and J. Fang, "Nanoparticle Attachment on Silver Corrugated-Wire Nanoantenna for Large Increases of Surface-Enhanced Raman Scattering," ACS Nano **5**(12), 9442–9449 (2011).
30. D. He, B. Hu, Q.-F. Yao, K. Wang, and S.-H. Yu, "Large-Scale Synthesis of Flexible Free-Standing SERS Substrates with High Sensitivity: Electrospun PVA Nanofibers Embedded with Controlled Alignment of Silver Nanoparticles," ACS Nano **3**(12), 3993–4002 (2009).
31. R. Alvarez-Puebla, B. Cui, J.-P. Barvo-Vasquez, T. Veres, and H. Fenniri, "Nanoimprinted SERS-active substrates with tunable surface plasmon resonances," J. Phys. Chem. C **111**(18), 6720–6723 (2007).

1. Introduction

Plasmonics are currently seeking widespread applications in the area of plasmonic surface-enahaned Raman scattering sensors [1–3], plasmonic lasers [4–6], surface-plasmon-enhanced light-emitting diodes [7], plasmonic light trapping [8–14], plasmonic integrated circuits [15,16], plasmonic imaging below diffraction limit [17], nanoscale plasmoinc waveguiding [18–21] and optical antennas [22]. All these applications require the extreme confinement of light and its related nonlinear effects which can be achieved by guiding and concentration light using plasmonic nanostructures. But the question is how to advantageously use Plasmon excitation and localization in all these opportunities. Therefore, a lot of research has been expanded in area for materials [11–14, 23,24], device geometries [25–29], nanoscale fabrication [30,31] and characterization to understand the behavior and ability of Plasmon which in turn open up developments and new approaches in nanophotonic application. As a result, in Surface Enhanced Raman Scattering (SERS) technology, enhancement is increased ten-fold through the use of plasmonic substrates. In photovoltaic devices, plasmonic metal

Optics EXPRESS

nanoparticles can be used either as efficient scatters or to enhance the generation of photo carriers through local field enhancement around the metal nanoparticles. Plasmonic waveguide have enabled transmission of light through holes smaller than its wavelength. Studies are just beginning to appear exploring contributions from plasmonic coupling. This paper investigates the effect of metal layer conformality on plasmon behavior for three dimensional arrays of inverted rectangular pyramidal pits. We observe that by tailoring the non-conformality of the gold coating it is possible to tune the absorption in the infrared (IR) wavelength range which might be useful for applications in silicon solar cells where broadband absorption over the IR range is challenging. In addition to that, a nano-textured metallic surface with a non-conformal metal coating can behave as an efficient broadband reflector.

2. Simulation and discussion of the nonconformal effect on plasmonic properties

2.1 Design and simulation

In numerical simulation of plasmonic substrates, it is difficult to calculate plasmon absorption bands directly. It is therefore wise to determine the diffraction efficiencies and the related electric field distributions given by a structure and then determine the plasmon dispersion bands from the data. There are numerous simulation methods such as finite-element simulation, finite difference time domain (FDTD), discrete-dipole approximation method and rigorous coupled wave analysis (RCWA) method which can be used to determine the diffraction efficiency.

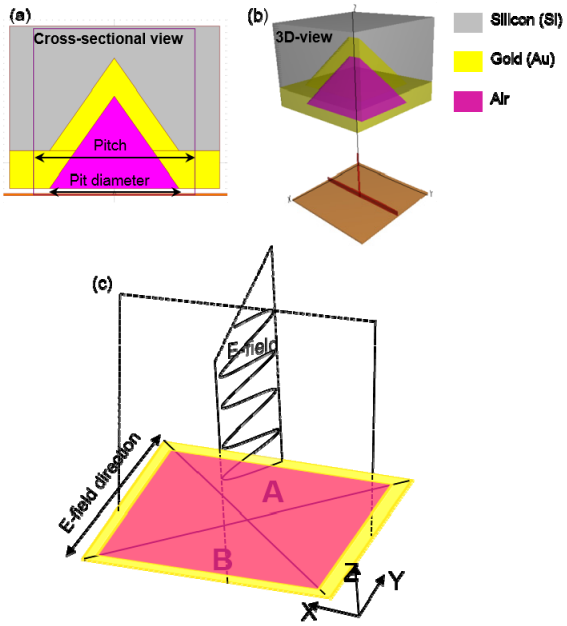

Fig. 1. Schematic diagrams of the modeled inverted rectangular pyramidal pit (a) cross-sectional view (b) 3-dimensional view and (c) diagram shows the electric field direction for TM polarization. “A” and “B” are labelled for the opposite sidewalls.

In this paper, an array of three dimensional inverted pyramid (rectangular lattice) is modeled using the RSoft ‘DiffractMOD’ based on RCWA method. This has been implemented using advanced algorithms including fast Fourier factorization and generalized transmission line formulation for boundary condition. RCWA method represents electromagnetic field as sum of coupled waves and uses complex periodic permittivity

Optics EXPRESS

functions for the material to avoid perfect conductor approximation which is applicable for microwave but leads to erroneous results for visible wavelengths. Figure 1 shows the definition of geometrical features, hereafter pitch length is denoted as "P" and pit size as "S". All the simulation results shown here are for rectangular pit unless otherwise stated. The simulation outcome of the DiffractMOD simulator is diffraction efficiency given by the pyramidal pit as a function of broadband excitation wavelength. The dispersion map is formed by plotting a group of numerical data related to diffraction efficiency as a function of incident angles over the broadband wavelength range, together as a single color map. In which, wavelength varies along y-axis, incident angle varies along x-axis and their respective diffraction efficiency is given in terms of color intensity (dark blue to dark red). Therefore, dark blue color denotes 100 percent plasmon absorption while the dark red represents complete reflection. The advantage of plotting data as a dispersion map is that it allows identification of diffraction, non-dispersive and dispersive plasmon modes. Generally, dispersive modes propagate over a metallic surface and its plasmon energies are highly dependent on incident angle and show up as sharp absorption modes. Non-dispersive plasmon modes predominantly trap their energy inside the pyramidal pit and its dispersion band is far broader than the dispersive (propagating) plasmon bands. The simple diffraction mode is related to the periodicity (pitch length). All simulations are run for TM polarization state unless otherwise stated. Understanding the polarization will help in the observation and understanding of the dispersion map and its relative electric field and plasmon properties. Figure 1(c) shows the top view of a pyramid indicating the variation of electric field (e-field vector) on the sidewalls for the TM polarization state in which the e-field is confined within the pits by the sidewall A and B resulting in higher e-field energy confinement in longer sidewall (YZ view).

2.2 Results and discussion

To study the non-conformal effect on plasmonic properties, the design for 780-800nm excitation (pyramidal pits 1250P1000S with Au200nm gold coating thickness) which has been demonstrated to show high SERS enhancement factor [3]. The measured pit size after glancing angle deposition shows 961nm instead of 1000nm in fabrication. Therefore, simulated pit size is designed as 961nm. Sample-1250P961S with the conformal metal coating is from now on defined as non-conformality"0". In this case sidewalls of the pits have a uniform coating of even thickness (170nm). We then change the taper factor for the sidewall coatings of the pits to simulate the effect of different angular deposition conditions. In the simulation we are therefore able to gradually increase the non-conformality of metallization. Gold coating thickness on the pit sidewalls at the top of the pyramids is varied in steps of 100nm, whilst maintaining the same gold coating thickness (170nm) at the bottom of the pits as shown in table1.

Table 1. List of pyramidal geometric data with 'apex angle decreased non-conformality' condition using the 1250nm pitch (1250P)

Degree of Non-conformality	0	1	2	3	4	5	6	7
pit size in nm (S)	961	861	761	661	561	461	361	261
Apex angle (θ)	70.6	62.74	56.63	50.16	43.33	36.15	28.68	20.94

In this case, the effective width of the neck of the pyramid decreases in proportion, and the apex angle of the pyramid decreased by the average value of 7° (shown in Table 1). In this paper, we define this type as 'apex angle decreased non-conformal' coating. Conversely we define 'backward non-conformal' coating to cause an increase in apex angle and pit neck diameter.

Optics EXPRESS

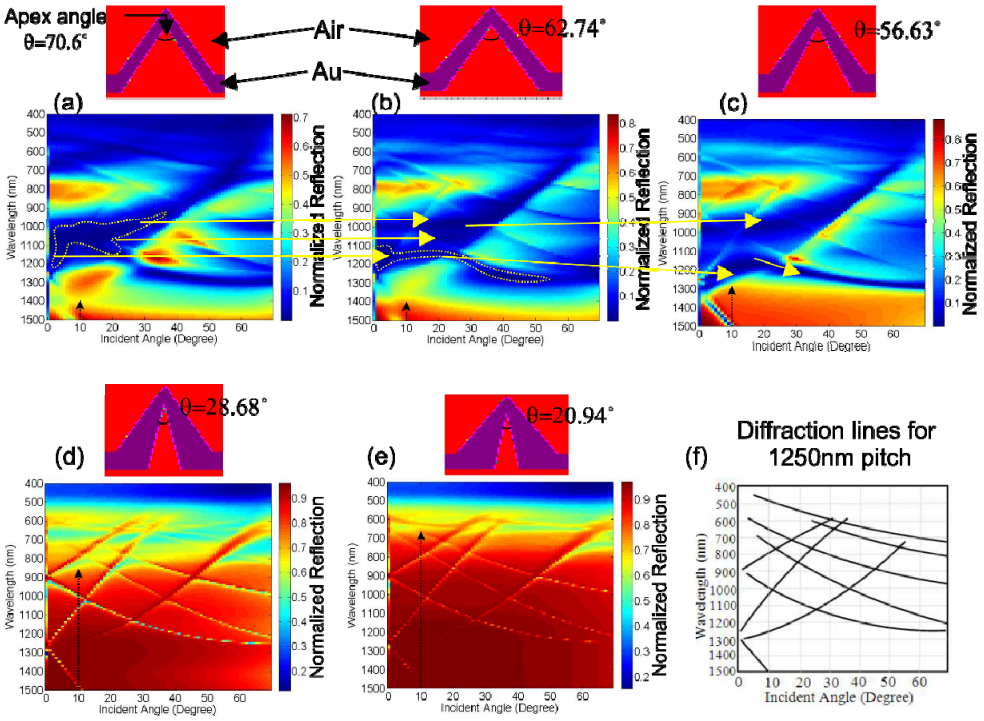

Fig. 2. Simulation results show the effect of non-conformal gold coating resulted from decrease in apex angle of pyramid. Upper image shows index profile indicating the change in apex angle, "θ". Lower images show the dispersion maps. Yellow arrows are indicating the evolution of Plasmon mode from broadband localized Plasmon shown by the dotted circle. Length of black dotted arrow indicates the region of high reflection. (a): θ = 70.6° (b) θ = 62.74° (c): θ = 56.63° Yellow arrow indicates the propagating plasmon modes resulted from the coupling of two localized plasmon modes from (b). (d) θ = 28.68° (e): θ = 20.94°. The series of black-dotted arrows (Fig. 2(a, b, c, d and e) show the gradual influence of reflection over the broad wavelength. (f): Plot of diffraction modes for all non-conformal gold coating designs fixed at 1250nm pitch length.

Figure 2 shows the results of index profiles and dispersion maps of the respective non-conformality condition. In figures of index profiles, the purple region is the gold coated area and red region is the air. Since the pitch length of the underlying pyramid (normally formed in silicon) is fixed at 1250nm, the diffraction behavior of all designs is same for the zero order diffraction mode as this is determined by pit to pit periodicity. Therefore, simple diffraction modes are not affected by the effect of conformality of metal coating (as shown in Fig. 2(f)). The change in the formation of gold coating can be seen more clearly in the index profile plots (upper in Figs. 2(a), 2(b), 2(c), 2(d), and 2(e)). Results presented in Figs. 2(a), 2(b), and 2(c)) show that gradual reduction in coating conformality directly affects localized plasmons confined within the pit in such a way that broadband localized plasmons (Fig. 2(a) – shown by white dotted circle) are split into either the narrower localized plasmon (Fig. 2(b) - shown by yellow arrows) or sharp propagating plasmons modes (Fig. 2(c) – short yellow arrow). The split plasmon band can again affect nearby plasmons' behavior and energy levels. The evolution of plasmon process can be seen briefly in the dispersion maps of noncon-0, 1and 2 shown by drawing of yellow arrows and white-dotted circles (Fig. 2(a), 2(b) and 2(c)). The arrows show the way plasmons split and the white-dotted circle indicates the evolved Plasmon. The detailed plasmon behavior relating to non-conformality effect is studied with the individual incident angle as shown in Fig. 3.

Optics EXPRESS

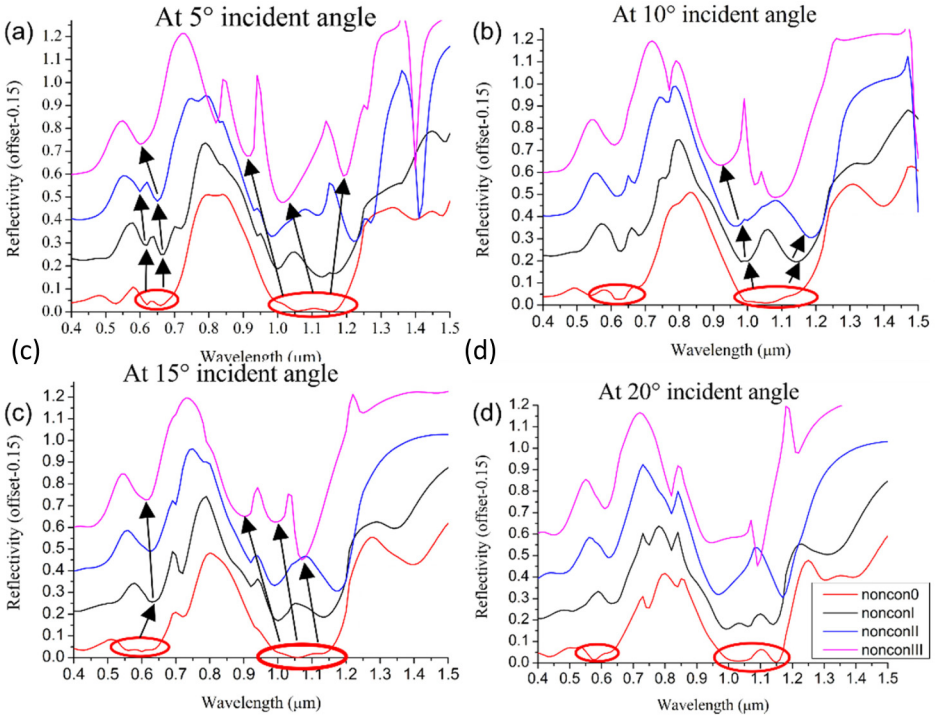

Fig. 3. Normalized Reflectivity spectra for non-conformal gold coating shows the changes in Plasmon behavior and its energy at (a) 5° incident angle (b) 10° incident angle (c) 15° incident angle (d) 20° incident angle.

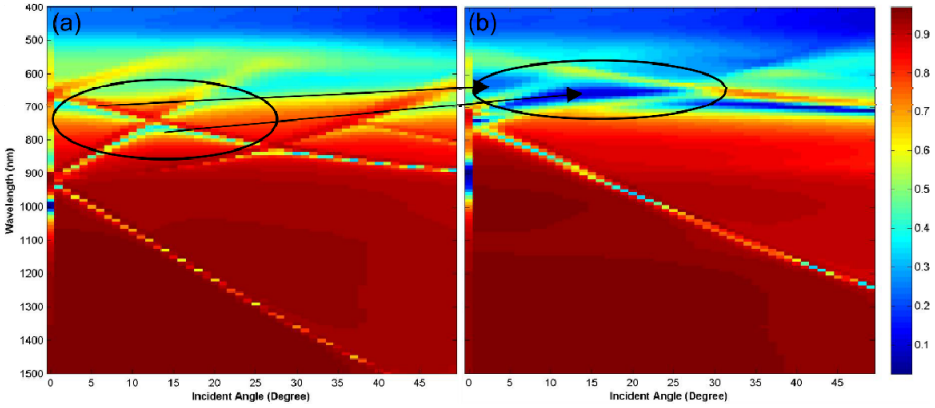

Fig. 4. Dispersion maps for reducing pith length by 200nm at noncon-7 condition at TM polarization (a) 900P261D (b) 700P261D

Figure 3 shows the normalized reflectivity spectra for a range of metal non-conformality for specific example incident angle of 5°, 10°, 15° and 20°. The fact that broadband localized plasmons are independent from the incident angle is observed and shown by red circle in Fig. 3(a), 3(b), 3(c), and 3(d) results for non-confromality '0'.When non-conformality changes, plasmons modes become shifted. In 600nm-700nm range and 950nm-1250nm range, the broadband localized plasmons become divided into 2 or three localized plasmon modes (as shown by black arrows in Figs. 3(a), 3(b) and 3(c) and plasmon absorption efficiencies are decreased to 80%-90% from 90%-99% corresponding to the effect of non-conformality. The high energy plasmon can be formed till noncon-4 ($\theta = 43.33°$) condition due to the limitation

Optics EXPRESS

of pitch length, the plasmons could not couple to incident and reflected photon in the higher forward non-conformality gold coating. Due to the reduced apex angle of the pyramid, instead of plasmon absorption high reflection are overtaken and shifted from 1500nm to 700nm range. Within the infrared region, reflection efficiency is achieved from 84% to 96% at noncon-7 condition (θ = 20.94°). Therefore, for the noncon-7 design reducing the pitch from 1250nm by 250nm and 200nm consecutively it is possible to harness the plasmon absorption in the visible and near infra-red region as well as high reflection in infra-red region. Figure 4(a) and 4(b) are the results of 900nm pitch-261nm pit and 700nm pitch-261nm pit, respectively. As we expected, the localized plasmons are gradually shifted to near infra-red region (600nm-700nm) and the plasmon energy also become stronger while maintaining the efficient broadband mirror-like reflection with wider angular spread in infrared region.

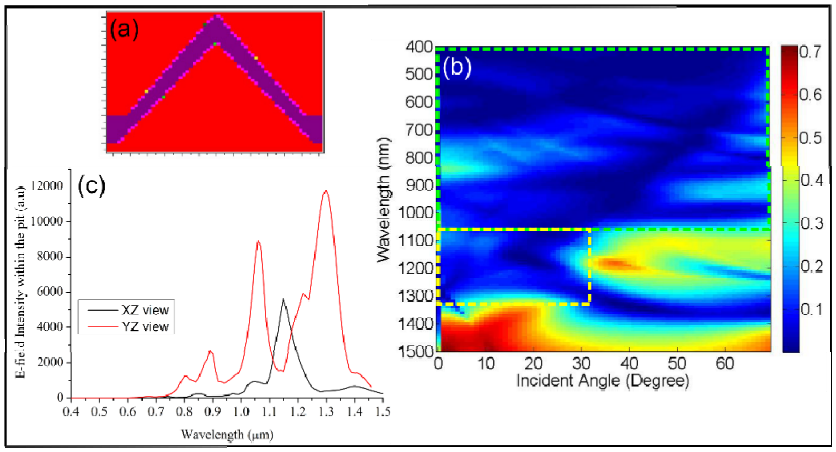

Fig. 5. Effect of apex angle increased non-conformality coating on plasmon properties: (a) index profile (b) dispersion map. Green box shows the high plasmon absorption over wide angular spectrum in visible and near infrared region and yellow box shows the high energy plasmons in part of infrared region. (c) e-field energy within the pit.

When the conformal coating is modified by the increasing the apex angle (θ = 78.5°) instead of decreasing it, the pit size becomes slightly larger to 1150nm with 1250nm pitch length as shown in Fig. 5(a). Interestingly, the higher plasmon energy modes are formed as wider angular spectrum over broadband wavelength (shown by green box) including most of the infrared region (shown by yellow box) as shown in Fig. 5(b). This large amount of plasmon confinement is partly due to the increased apex angle and larger pit size formed by non-conformally. Moreover, in the simulation the e-field energy within the pit is observed by two monitors: one for XZ view and other for YZ view, Fig. 5(c). Both monitors show that high energy is trapped within the pit over the infra-red wavelength range although e-field is larger in YZ view due to the TM incident polarization state.

3. Conclusion

This paper studies the effect of non-conformality of gold coating (due to angled deposition) on behavior of surface plasmons for SERS enhancing inverted pyramidal pit arrays. Non-conformal metal coating affects the pit diameter and shape which in turn affect surface plasmon, resonance and energy. Two types of geometries are defined (‘decreased and increased apex angle’ non-conformal coating). The former makes the pit diameter smaller at the top resulting in thinner metal thickness at the region near the tip of the pyramid after metal coating. The Latter causes a thicker metal at the region near the tip of the pyramid. In ‘decreased apex angle’ non-conformal coating, wider broadband localized plasmon separated into narrower localized plasmon bands with lower plasmon energy. Therefore broadband

Optics EXPRESS

reflection is more efficient over the near-infrared and infrared region. After fixing the pitch length to 900nm and 700nm, the high plasmon absorption energy is appointed in the near-infrared region while the efficient wider reflection spectrum is in infrared region. In 'increased apex angle' non-conformal coating, the plasmonic energy is higher and the plasmonic bands are preferentially wider and occupy in the visible, near-infrared and part of the infrared region of the spectrum. Understanding the effect of metal layer conformality on plasmon dispersion provides the clear insight into how to further improve SERS enhancement factor in sensing applications. Moreover, dependent upon conformality of the gold coating the nano-textured metallic surface could be suitable to act either as an efficient broadband mirror-like reflector or as an efficient broadband, wide angle absorber at infrared wavelengths. Creation of a broadband wide angle absorbing surface such as this has important implications for photovoltaic cells.

Funding

EPSRC grant (RP014154).